MODELING OF THE REYNOLDS STRESS IN THE BURSTING LAYER AFFECTED BY TYPHOON

Tomokazu Murakami[1], Jun Yoshino[2] and Takashi Yasuda[2]

When large and intensive water surface displacements are caused by developed wind waves due to a typhoon, it is impossible in the Eulerian coordinate system to measure water particle velocities continuously in a domain between the wave trough level and the mean water level. Consequently, the domain between the wave trough level and the mean water level becomes a void zone where the Reynolds stress cannot be described. By treating the sea surface boundary layer including the void zone as a bursting layer, we modeled the Reynolds stress in the bursting layer. Validity of that modeling was verified by performing comparisons with experimentally obtained results.

Keywords: Reynolds stress; sea surface boundary layer; wind-wave breakers; turbulence modeling

INTRODUCTION

Correct descriptions of the Reynolds stress in a sea surface boundary layer generated by strong the winds of a typhoon are extremely important for highly accurate predictions of typhoon intensity and transportation phenomena of surface waters affected by the typhoon because latent heat fluxes characterizing the typhoon intensity and velocity fields determining the amount of sea surface transportation are dominated by the Reynolds stress in the layer (Skachko et al. 2009; Ogasawara and Yasuda 2004).

The Reynolds stress in the sea surface boundary layer is described by application of the Reynolds average rule based on the assumption of the averaged sea surface to velocity fields in the layer. However, waves generated by strong winds of the typhoon produce large vertical displacements of the water surface that might exceed 20 m. In the Eulerian coordinate system, it is impossible to measure water particle velocities continuously in a domain between the wave trough level (WTL) and the mean water level (MWL) because of the large water-surface displacement. Consequently, the Reynolds average rule is inapplicable to velocity fields above the WTL. The domain between the wave trough level and the mean water level therefore becomes a void zone where the Reynolds stress cannot be described.

Although the sea surface boundary layer including the void zone is extremely important for determination of the typhoon intensity and transportation phenomena in the sea surface affected by the typhoon, conventional models (Craig and Banner 1994; Mellor and Blumberg 2004) using the Reynolds equation treat the sea surface boundary layer including the void zone as an unresolved zone with thickness defined as roughness length z_0 (Soloviev and Lukas 2006).

Furthermore, the sea surface affected by strong winds becomes covered with developed wind-wave breakers. The turbulent flow fields in the sea surface boundary layer comprise a mixture of the mean flow, the cascade turbulence from the mean flow, the wave motion, and the turbulence generated by wave-breaking and airflow separation. Therefore, the Boussinesq eddy viscosity assumption, which is used in conventional models described above, becomes insufficient to describe all the turbulent components in the sea surface boundary layer.

In this study, an experiment using a double-bottomed wind-wave tank (Ogasawara and Yasuda 2004) is performed to obtain information related to the total mass flux, the vertical distribution of the mean flow velocity and the turbulent flow components affected by strong winds, which are required to describe the Reynolds stress. The sea surface boundary layer including the void zone is treated as the bursting layer, which is defined as a boundary layer affected by various actions such as wave breaking, airflow separation, and air bubbles, using a macroscopic approach to the assumption of the averaged sea surface (Murakami and Yasuda 2008). Then, the Reynolds average rule is applied to the velocity fields in the bursting layer. Furthermore, the Reynolds stress in the bursting layer is separated into a low-frequency Reynolds stress that originates from the mean shear flow and a high-frequency Reynolds stress that originates from the overall breaker action based on the experimental results. Finally, the bursting-layer model is developed to enable description of the low-frequency Reynolds

[1] Storm, Flood, and Landslide Research Department, National Research Institute for Earth Science and Disaster Prevention, 3-1, Tennodai, Tsukuba, Ibaraki, 305-0006, Japan
[2] Environmental and Renewable Energy Systems Division, Graduate School of Engineering, Gifu University, 1-1 Yanagido, Gifu, 501-1193, Japan

stress and the high-frequency Reynolds stress in the bursting layer (i.e. the domain of roughness length z_0). The model validity is verified through comparison with experimental results.

MODELING CONCEPT

The void zone described above originates from the procedure by which the actual space is converted into an averaged space (bursting layer) based on the Reynolds average rule. It is necessary that the modeling to determine the vertical distribution up to the MWL of the mean velocity $\overline{u}$ in the averaged space. Ogasawara and Yasuda (2004) showed that the value of the total mass flux q_A can be determined using a double-bottomed wind-wave tank. If the value of q_A is known, then the value up to the MWL of the horizontal velocity $\overline{u}$ can be determined to satisfy the following equation.

$$q_A = \int_{-h}^{0} \overline{u} dz \tag{1}$$

In that equation, h is defined as a distance from the mean water level to the upper bottom in the wind-wave tank with a double bottom.

The solution of the Reynolds equation in the bursting layer must agree with the value of $\overline{u}$. Based on this consideration, the Reynolds stress is formulated by giving the vertical distribution up to MWL of $\overline{u}$ as the solution of the Reynolds equation in the bursting layer, and by then solving that equation as an inverse problem. Therefore, the modeling in this study is distinguished as a macroscopic approach based on information related to the vertical distribution of the horizontal mean velocity.

EXPERIMENTS

Laboratory experiments were performed using a 15.4-m-long, 0.4-m-wide, and 1.0-m-deep double-bottomed wind-wave tank, as illustrated in Fig. 1. The tank partially fulfills the continuity of the mass flux and reduces the influence of the return flow on wind-driven currents. The space between the upper and lower bottoms of the tank functions as a duct to circulate the currents as a return flow, allowing measurement of the return-flow velocity, which is only disturbed by the reverse pressure gradient within the tank. Therefore, the true wind-driven current, resulting solely from wind stress, is measurable according to the velocity of this measured return flow (Ogasawara and Yasuda 2004).

The still water depth was fixed as 60 cm. Reference wind speed U_r at the wind-tunnel entrance is set as 12.0 m/s, yielding fully breaking waves. Table 1 presents values of wave parameters at measuring point W03, where H_s is the significant wave height, T_s is the significant wave period, and f_p denotes the peak frequency of the wave spectrum. The friction wind velocity u_{*a} was calculated using the empirical equation proposed by Wu (1980). Water particle velocity fields were visualized using 50-μm-diameter nylon particles and a relative density of 1.02 as tracers. Nylon particles were irradiated from the tank floor using a 5-mm-thick 5 W power green light laser sheet. Images showing their positions were captured using two synchronized cameras of 480 × 480 pixel resolution at a 125 fps rate. The resultant images facilitated measurement of high-speed velocity fields immediately below the WTL. Velocity fields were examined using a high-resolution PIV system (Ogasawara et al. 2002), which can analyze high-speed and intensively fluctuating water particle velocities that are affected by breaking waves.

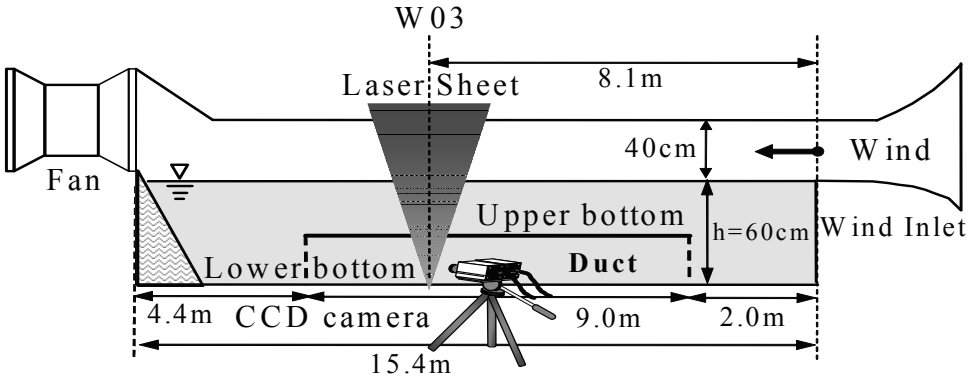

Figure 1. Wind-wave tank with a double bottom.

Table 1. Wave parameters at measuring location W03.

U_r (m/s)	u_{*a} (m/s)	H_s (cm)	T_s (s)	f_p (Hz)
12.0	0.48	7.46	0.58	1.73

LOW AND HIGH-FREQUENCY REYNOLDS STRESSES

Velocity components of currents driven by strong winds comprise a mixture of the mean flow, the cascade turbulence from the mean flow (low-frequency turbulence), the wave motion, and the turbulence generated by breaking waves (high-frequency turbulence), as apparent from the shape of the velocity spectrum presented in Fig. 2. To model the breaker stresses that cause the bursting layer, it is necessary to extract the breaker-generated turbulence from the mixture of these turbulent flow components. Thereby, three cutoff frequencies are provided from the shape of the velocity spectrum presented in Fig. 2: f_{cc} between the spectral band of the mean flow and the low-frequency turbulence; f_{lc} between the low-frequency turbulence and the wave motion; and f_{hc} between the wave motion and high-frequency turbulence. Based on them, the spectral band is separable into four domains. Velocities $\mathbf{u}$ of currents driven by strong winds are treated as the sum of the mean flow velocity $\mathbf{u}_c$, the cascade turbulence velocity $\mathbf{u}_l$, the wave motion velocity $\mathbf{u}_w$, and the velocity of the breaker-generated turbulence $\mathbf{u}_h$:

$$\mathbf{u} = \mathbf{u}_c + \mathbf{u}_l + \mathbf{u}_w + \mathbf{u}_h \,. \tag{2}$$

The mutual correlations among components must be known when the Reynolds average rule is applied to these components. The reverse-Fourier transform is then performed to investigate the values of the correlation coefficients between each velocity component. Table 2 presents experimental values of the correlation tensor among horizontal and vertical velocity components at depths of z = -3, -6, and -10 cm for respective frequency bands. Results show that the value of the cross-correlation between the velocity components in different frequency bands is of negligible order at each water depth. Even for breaker-affected velocity fields comprising a mixture of various turbulent flow components with different origins, only components in the same frequency band of the correlation tensor have considerable values. Thereby, the following Reynolds average rule becomes applicable.

$$\overline{u} = u_c \tag{3}$$

$$\overline{u_l} \quad , \quad \overline{u_w} \quad , \quad \overline{u_h} = 0 \tag{4}$$

$$\overline{u_c u_l} \quad , \quad \overline{u_c u_w} \quad , \quad \overline{u_c u_h} = 0 \tag{5}$$

$$\overline{u_l u_w} \quad , \quad \overline{u_l u_h} = 0 \tag{6}$$

$$\overline{u_w u_h} = 0 \tag{7}$$

$$\overline{u^2} = \overline{u_c^{\,2}} + \overline{u_l^{\,2}} + \overline{u_w^{\,2}} + \overline{u_h^{\,2}} \tag{8}$$

Furthermore, the averaging rule below can apply to the cross-correlation term $-\overline{uw}$, as Table 2 shows.

$$-\overline{uw} = -\overline{u_l w_l} - \overline{u_w w_w} - \overline{u_h w_h} \tag{9}$$

In that equation, $-\overline{u_l w_l}$ is the low-frequency Reynolds stress, which can be described by the following Boussinesq eddy viscosity assumption because $-\overline{u_l w_l}$ originates from the mean shear flow.

$$-\overline{u_l w_l} = \nu_l \frac{\partial \overline{u}}{\partial z} \tag{10}$$

Here, ν_l is a low-frequency eddy viscosity coefficient, which is generated only by the mean shear flow.

Because the orthogonal relation holds between u_w and w_w of the irrotational wave, their inner product $-\overline{u_w w_w}$ becomes 0. However, the actual value of the inner product is not negligible; rather it is significant because $-\overline{u_w w_w}$ comprises the turbulence generated by wave-breaking, the cascading turbulence from mean shear flow and rotational wave motion. Their primary energy source is presumed to be waves and breakers generated by strong winds in addition to that of $-\overline{u_h w_h}$. Therefore, $-\overline{u_w w_w}$ and $-\overline{u_h w_h}$ are superposed and treated collectively as the high-frequency Reynolds stress $-\overline{u_t w_t}$ caused by wave and higher-frequency turbulence and are represented as

$$-\overline{u_t w_t} = -\overline{u_w w_w} - \overline{u_h w_h} \, . \tag{11}$$

The total Reynolds stress $-\overline{uw}$ in the bursting layer is balanced with the momentum flux by the strong winds. The following relation holds for all depths in the bursting layer under the assumption of the constant flux layer.

$$-\overline{uw} = -\overline{u_l w_l} - \overline{u_t w_t} = u_*^{\,2} \quad : z = -z_0 \sim 0 \tag{12}$$

Consequently, the high-frequency Reynolds stress $-\overline{u_t w_t}$ is represented as

$$-\overline{u_t w_t} = u_*^{\,2} - \nu_l \frac{\partial \overline{u}}{\partial z} \, . \tag{13}$$

Equations (10) and (13) show that the low-frequency Reynolds stress $-\overline{u_l w_l}$ and the high-frequency Reynolds stress $-\overline{u_t w_t}$ are describable by the formulation of the vertical distribution up to the MWL of the mean velocity $\overline{u}$ and the value of the low-frequency eddy viscosity coefficient ν_l.

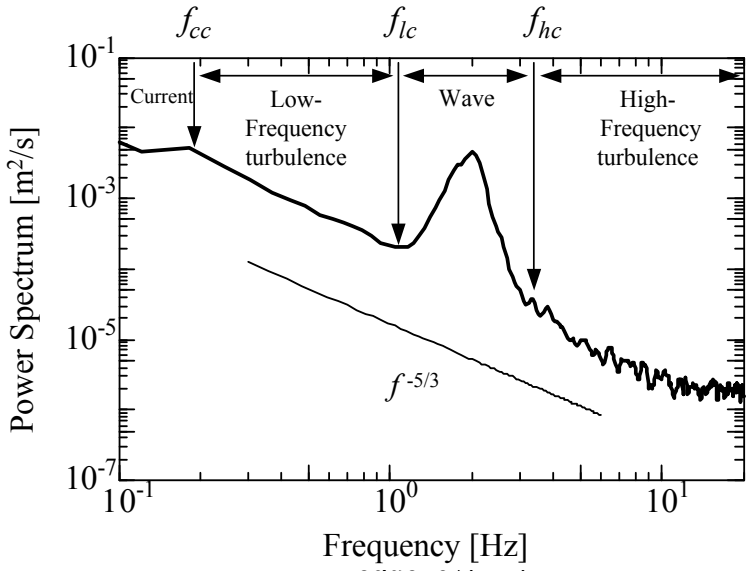

Figure 2. Division of frequency bands of the velocity spectrum (mean velocity, low-frequency turbulence, wave motion, and high-frequency turbulence).

Table 2. Values of correlation tensors among the horizontal and vertical velocity components at depths of *z* = -3, -6, and -10 cm in each frequency band at wind speed of 12.0 m/s.

$z(cm)$	$\overline{u_c^2}$	$\overline{u_c u_l}$	$\overline{u_c u_w}$	$\overline{u_c u_h}$	$\overline{u_c w_l}$	$\overline{u_c w_w}$	$\overline{u_c w_h}$
-3	7.59×10^{-3}	1.50×10^{-19}	3.34×10^{-20}	1.39×10^{-21}	-1.70×10^{-20}	1.64×10^{-20}	-6.26×10^{-22}
-6	2.18×10^{-3}	7.88×10^{-20}	3.06×10^{-20}	-3.78×10^{-21}	-1.77×10^{-19}	1.30×10^{-20}	6.41×10^{-21}
-10	2.23×10^{-3}	-3.38×10^{-20}	-9.50×10^{-21}	2.19×10^{-21}	3.82×10^{-20}	-1.05×10^{-20}	1.12×10^{-21}

$z(cm)$	$\overline{u_l^2}$	$\overline{u_l w_l}$	$\overline{u_l u_w}$	$\overline{u_l u_h}$	$\overline{u_l w_w}$	$\overline{u_l w_h}$
-3	1.60×10^{-3}	-4.27×10^{-4}	-3.32×10^{-21}	4.51×10^{-21}	-2.09×10^{-20}	-2.52×10^{-21}
-6	1.23×10^{-3}	-3.59×10^{-4}	-9.38×10^{-21}	-3.31×10^{-21}	-1.53×10^{-21}	-2.47×10^{-21}
-10	7.06×10^{-4}	-7.64×10^{-5}	-2.15×10^{-20}	5.59×10^{-22}	9.87×10^{-21}	5.58×10^{-22}

$z(cm)$	$\overline{u_w^2}$	$\overline{u_w w_w}$	$\overline{u_w u_h}$	$\overline{u_w w_l}$	$\overline{u_w w_h}$
-3	8.15×10^{-3}	4.03×10^{-4}	1.10×10^{-20}	-1.23×10^{-20}	-8.79×10^{-22}
-6	6.68×10^{-3}	2.47×10^{-4}	-1.00×10^{-21}	-1.10×10^{-20}	1.38×10^{-21}
-10	3.29×10^{-3}	9.75×10^{-5}	6.40×10^{-21}	-2.08×10^{-20}	-6.34×10^{-21}

$z(cm)$	$\overline{u_h^2}$	$\overline{u_h w_h}$	$\overline{u_h w_l}$	$\overline{u_l w_w}$
-3	9.37×10^{-4}	-1.17×10^{-4}	1.78×10^{-21}	-3.18×10^{-22}
-6	2.25×10^{-4}	-1.14×10^{-5}	4.49×10^{-21}	-1.16×10^{-20}
-10	8.34×10^{-5}	-4.26×10^{-6}	-2.14×10^{-21}	5.72×10^{-22}

VERTICAL DISTRIBUTION OF THE HORIZONTAL MEAN VELOCITY

The vertical distribution up to the MWL of the mean velocity $\overline{u}$ is determined to make its vertically integrated value agree with the total mass flux of the wind-driven currents obtained from our experiments. The value and the vertical distribution of the modeled formulation must correspond to those of the following logarithmic law at the interface between the bursting layer and the logarithmic-law layer ($z = -z_0$).

$$\overline{u} = \overline{u_b} - \frac{u_*}{\kappa}\log\left(\frac{-z}{z_0}\right) \tag{14}$$

In that equation, κ represents von Karman's constant; $\overline{u_b}$ is the value of mean velocity at $z = -z_0$.

Because the breaker turbulence is nonexistent in the logarithmic-law layer ($z \le -z_0$), the high-frequency Reynolds stress of Eq. (13) is zero at $z = -z_0$. In addition, the eddy viscosity coefficient ν in the logarithmic-law layer is represented based on the mixing length theory as

$$\nu = -\kappa u_* z \ . \tag{15}$$

The value of the eddy viscosity coefficient ν at $z = -z_0$ is identical to the low-frequency eddy viscosity coefficient ν_l. Therefore, substitution of Eq. (15) into Eq. (13) yields the following relation.

$$u_*^{\,2} + \kappa u_* z \frac{\partial \overline{u}}{\partial z} = 0 \quad \text{on} \ \ z = -z_0 \tag{16}$$

Based on these conditions, the vertical distribution up to the MWL of the mean velocity $\overline{u}$ is modeled as

$$\overline{u} = \overline{u_b} + \frac{u_*}{\kappa}\exp\left(\frac{-z}{z_0}\right) - \frac{u_*}{\kappa} + \alpha\frac{u_*}{\kappa}\left(\frac{z_0+\gamma}{-z+\gamma}\right)^{\beta} . \tag{17}$$

$$\alpha = 44.72 \ , \ \beta = 2.01 \ , \ \gamma = 0.37$$

In those equations, α , β , and γ signify dimensionless constants. Their values are determined to make the vertically integrated value of Eq. (17) agree with the total mass flux measured in the experiment.

LOW-FREQUENCY EDDY VISCOSITY COEFFICIENT

The low-frequency Reynolds stress $-\overline{u_l w_l}$ originates from the mean shear flow. Therefore, the following relation of the mixing length theory holds in the bursting layer.

$$-\overline{u_l w_l} = l^2\left(\frac{\partial \overline{u}}{\partial z}\right)^2 \tag{18}$$

Substitution of Eq. (18) into Eq. (10) yields the low-frequency eddy viscosity coefficient ν_l , which is represented as

$$\nu_l = l^2\frac{\partial \overline{u}}{\partial z} \ . \tag{19}$$

The length scale l of the low-frequency turbulences is limited by the distance from the sea surface because the sea surface is treated virtually as a rigid lid at the MWL. Thereby, we assumed that the wall-law holds in the layer and employed the mixing length theory of $l = -\kappa z$ to calculate the low-frequency eddy viscosity coefficient ν_l in the bursting layer.

Figure 3 presents a comparison of the vertical distribution of the low-frequency eddy viscosity coefficient ν_l between the computational result obtained using the aforementioned procedure and the experimental one. Results show that the calculated values agree with the experimental ones.

Consequently, we infer that the assumption of the mixing length theory is applicable to the calculation of the low-frequency eddy viscosity coefficient ν_l in the bursting layer.

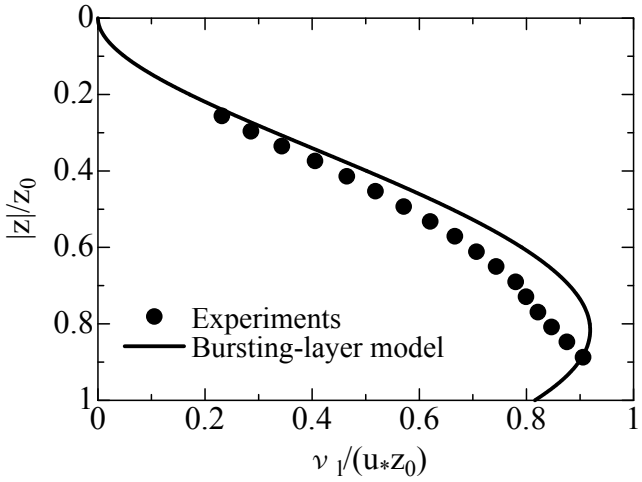

Figure 3. Comparison between computational results and experimental results obtained for the vertical distribution of the low-frequency eddy viscosity coefficient ν_l .

CALCULATION REPRODUCING EXPERIMENTAL VALUES OF THE LOW AND HIGH-FREQUENCY REYNOLDS STRESSES

Figure 4 presents a comparison of the vertical distribution of the low-frequency Reynolds stress $-\overline{u_l w_l}$ and the high-frequency Reynolds stress $-\overline{u_t w_t}$ between the computational results and the experimental ones. Results show that the bursting-layer model can describe the vertical distribution of $-\overline{u_l w_l}$ and $-\overline{u_t w_t}$ in the aforementioned void zone ($|z|/z_0 \geq 0.2$). Moreover, the vertical distributions of $-\overline{u_l w_l}$ and $-\overline{u_t w_t}$ given by the model in the zone $|z|/z_0$ = 1 to 0.2 agree well with the experimental distributions.

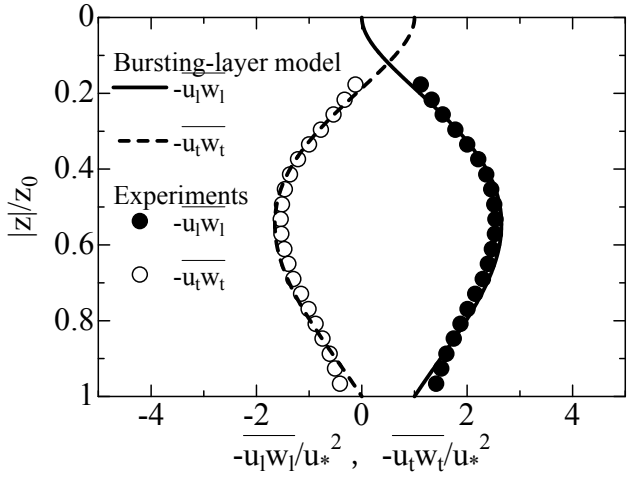

Figure 4. Comparison between computational results and experimental results obtained for the vertical distribution of low-frequency Reynolds stress $-\overline{u_l w_l}$ and the high-frequency Reynolds stress $-\overline{u_t w_t}$.

CALCULATION REPRODUCING EXPERIMENTAL VALUES OF THE HORIZONTAL MEAN VELOCITY

Calculations that are used to reproduce wind-driven currents in experiments are performed next. Those results are then compared to measured values to verify that the modeling of the bursting layer is performed appropriately.

The fundamental equations are the following continuity equation and bursting layer Reynolds equations in the vertically two-dimensional domain.

$$\frac{\partial \overline{u}_j}{\partial x_j} = 0 \tag{20}$$

$$\frac{\partial \overline{u}_i}{\partial t} + \overline{u}_j \frac{\partial \overline{u}_i}{\partial x_j} = -\frac{1}{\rho}\frac{\partial \overline{p}}{\partial x_i}\left(P + \frac{2}{3}k \right) + \frac{\partial}{\partial x_j}\left\{ (\nu + \nu_t)\left(\frac{\partial \overline{u}_i}{\partial x_j} + \frac{\partial \overline{u}_j}{\partial x_i} \right) \right\} + \mathbf{g} + \overline{\mathbf{D_b}} \tag{21}$$

$$\overline{D_{b\,i}} = \frac{\partial}{\partial z}\left[{u_*}^2 - (\kappa z)^2 \bullet \left\{ \frac{u_*}{\kappa z_0}\exp\left(1 + \frac{z}{z_0} \right) + \frac{\alpha u_*}{\kappa}\beta \left\{ \frac{\gamma + z_0}{-z + \gamma} - 1 \right\}^{\beta - 1} \bullet \frac{\gamma + z_0}{(-z + \gamma)^2} \right\} \right] \tag{22}$$

$$\overline{D_{b\,j}} = 0 \tag{23}$$

In those equations, k stands for turbulent kinetic energy, P represents pressure, and $\mathbf{g}$=(0,-g) and $\overline{\mathbf{D_b}}$ correspond to the high-frequency Reynolds stress $-\overline{u_t w_t}$.

The eddy viscosity coefficient that is necessary to represent the Reynolds stress resulting from the mean shear flow in Eq. (21) is obtained by solving the following k - ε turbulence model.

$$\nu_t = C_\mu \frac{k^2}{\varepsilon} \tag{24}$$

$$\frac{\partial k}{\partial t} + \overline{u}_j \frac{\partial k}{\partial x_j} = P_k - \varepsilon + \frac{\partial}{\partial x_j}\left\{ \left(\frac{\nu_t}{\sigma_k} + \nu \right)\frac{\partial k}{\partial x_j} \right\} \tag{25}$$

$$\frac{\partial \varepsilon}{\partial t} + \overline{u}_j \frac{\partial \varepsilon}{\partial x_j} = (C_{\varepsilon 1} P_k + C_{\varepsilon 2}\varepsilon)\frac{\varepsilon}{k} + \frac{\partial}{\partial x_j}\left\{ \left(\frac{\nu_t}{\sigma_\varepsilon} + \nu \right)\frac{\partial \varepsilon}{\partial x_j} \right\} \tag{26}$$

In those equations, P_k is the shear production term, defined as

$$P_k = \frac{\nu_t}{2}\left(\frac{\partial \overline{u}_i}{\partial x_j} + \frac{\partial \overline{u}_j}{\partial x_i} \right)\left(\frac{\partial \overline{u}_i}{\partial x_j} + \frac{\partial \overline{u}_j}{\partial x_i} \right). \tag{27}$$

Moreover, the standard values of C_μ = 0.09, σ_k = 1.0, σ_ε = 1.3, $C_{\varepsilon 1}$ = 1.44, and $C_{\varepsilon 2}$ = 1.92 are used as experimental constants.

Discrimination of these equations is performed using the finite difference method, which uses a staggered grid. Their solutions are obtained using the SOLA method (Hirt et al. 1976). The calculation domain is assumed to be of the same scale as that of the double-bottomed wind-wave tank (Fig. 1) used in the experiment; the lower duct was installed, as in the experiment. In that calculation, the time-step is set as 0.001 s, the horizontal resolution as 0.3 m, and the vertical resolution as 0.025 m. The initial state is assumed to be still water. Calculation of the wind-driven current is performed until it approaches the steady state. Calculated values of the horizontal velocity of the current are compared with the experimental ones at the same location W03 as those derived through the experiment.

Figure 5 presents a comparison of the vertical distribution of the horizontal mean velocity $\overline{u}$ between the computational result obtained using the bursting-layer model and the experimental one. Moreover, the vertical distribution of $\overline{u}$, calculated using a model proposed by Craig and Banner (1994), is also presented in Fig. 5. The Craig–Banner model is incapable of describing the steep vertical distribution in the bursting layer. In contrast, the bursting-layer model accurately calculated the steep vertical distribution of the current velocity in the bursting layer. This result demonstrates that both the modelings of the low-frequency Reynolds stress $-\overline{u_l w_l}$ and the high-frequency Reynolds stress $-\overline{u_t w_t}$ in the bursting layer are appropriate.

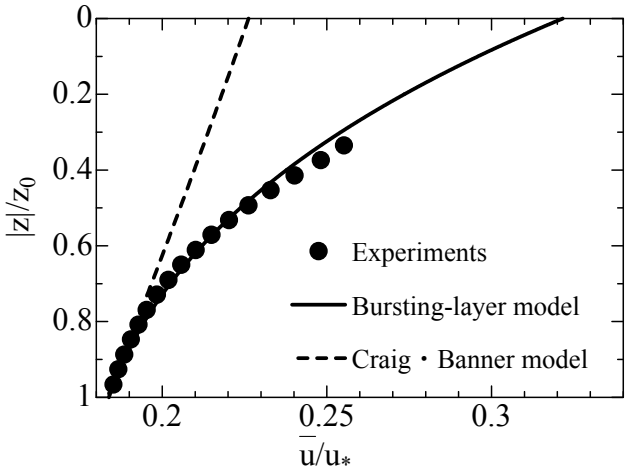

Figure 5. Comparison of the vertical distribution of the horizontal mean velocity $\overline{u}$ between experimental results and computational results obtained using the bursting-layer model the Craig–Banner model (1994).

CONCLUSIONS

This study was aimed at modeling of the Reynolds stress in the sea surface boundary layer including the void zone for cases in which the Reynolds stress cannot be described in the conventional models. The sea surface boundary layer was treated here as the bursting layer affected by various actions, such as wave breaking, airflow separation and air bubbles, and was modeled by describing their effects from a macroscopic viewpoint. Our experimental results demonstrated that the Reynolds stress in the bursting layer is separable into low-frequency Reynolds stress that originates from the mean shear flow and high-frequency Reynolds stress that originates from the overall breaker action.

Based on the concept of the bursting layer and the experimental results, we modeled the low-frequency Reynolds stress and the high-frequency Reynolds stress in the bursting layer. Validity of the modeling was verified through comparisons with experimental results. This model enables us to describe the vertical distributions of the Reynolds stress and the horizontal mean velocity in the sea surface boundary layer, regarded to have a thickness of roughness length z_0, which is treated in conventional models as the unresolved zone.

ACKNOWLEDGMENTS

This research was supported by a Grant-in-Aid for Scientific Research 21360234 from JSPS and the National Research Institute for Earth Science and Disaster Prevention through a research project on long-term prediction of typhoons and their accompanying disasters.

REFERENCES

Craig, P.D., and M.L. Banner. 1994. Modeling wave-enhanced turbulence in the ocean surface layer, *J. Phys. Oceanogr.,* 24, 2546–2559.

Hirt, C.W., B.D. Nichols, and N.C. Romero. 1975. SOLA-A numerical solution algorithm for transient fluid flows, *Los Alamos Scientific Laboratory Report*, LA-5852.

Mellor, G.L., and A.F. Blumberg. 2004. Wave breaking and ocean surface layer thermal response, *J. Phys. Oceanogr.,* 34, 693–698.

Murakami, T., and T. Yasuda. 2008. Bursting-Layer Modeling Based on the Assumption of the Averaged Sea Surface for Strong Wind-Driven Current, *J. Phys. Oceanogr.,* 38, 896–908.

Ogasawara, T., and T. Yasuda. 2004. Mass flux and vertical distribution of currents caused by strong winds in a wave tank, *J. Phys. Oceanogr.,* 34, 2712–2720.

Ogasawara, T., T. Yasuda and M. Takeda. 2002. Roles of wind wave breakers in momentum transfer processes from wind to currents and turbulence, *Proc. 12th Int. Offshore & Polar Eng. Conf.,* 85–91.

Skachko, S., J.M. Brankart, B.F. Castruccio, P. Brasseur, and J. Verron. 2009. Improved Turbulent Air-Sea Flux Bulk Parameters for Controlling the Response of the Ocean Mixed Layer: A Sequential Data Assimilation Approach, *J. Atmos. Oceanic Technol.*, 26, 538–555.

Soloviev, A., and R. Lukas. 2006. *The Near-Surface Layer of the Ocean: Structure, Dynamics and Applications*, Springer, 144–217.

Wu, J. 1980. Wind-stress coefficients over sea surface near neutral conditions, *J. Phys. Oceanogr.,* 10, 727–740.